

# A Sample of Clusters of Extragalactic Ultra Compact H II Regions

Kelsey E. Johnson

*JILA, University of Colorado and National Institute for Standards and Technology; and  
Department of Astrophysical and Planetary Sciences, Boulder, CO 80309-0440*

kjohnson@colorado.edu

Henry A. Kobulnicky

*Department of Astronomy, University of Wisconsin, 475 N. Charter St., Madison, WI  
53706*

chip@astro.wisc.edu

Philip Massey

*Lowell Observatory, 1400 Mars Hill Road, Flagstaff, AZ 86001*

massey@lowell.edu

and

Peter S. Conti

*JILA, University of Colorado and National Institute for Standards and Technology; and  
Department of Astrophysical and Planetary Sciences, Boulder, CO 80309-0440*

pconti@jila.colorado.edu

Draft of 30 May 2001

## ABSTRACT

We report on the detection of optically thick free-free radio sources in the galaxies M33, NGC 253, and NGC 6946 using data in the literature. We interpret these sources as being young, embedded star birth regions, which are likely to be clusters of ultracompact H II regions. All 35 of the sources presented in this article have positive radio spectral indices ( $\alpha > 0$  for  $S_\nu \propto \nu^\alpha$ ), suggesting an optically thick thermal bremsstrahlung origin from the H II region surrounding the hot stars. The estimated emission measures for these sources are  $EM_{6cm} \gtrsim 10^8 \text{ cm}^{-6} \text{ pc}$ , and energy requirements indicate that the sources in our sample have

a range of a few to  $\sim 560$  O7V star equivalents powering their HII regions. Assuming a Salpeter IMF with lower and upper mass cutoffs of 1 and  $100 M_{\odot}$ , respectively, this range in  $N_{Ly\alpha}$  corresponds to integrated stellar masses of  $0.1\text{--}60 \times 10^3 M_{\odot}$ . For roughly half of the sources in our sample, there is no obvious optical counterpart, giving further support for their deeply embedded nature; for most of the remaining sources the correspondance to an optical source is insecure due to relative astrometric uncertainty. Their luminosities and radio spectral energy distributions are consistent with HII regions modeled as spheres of plasma with electron densities from  $n_e \sim 1.5 \times 10^3$  to  $n_e \sim 1.5 \times 10^4 \text{ cm}^{-3}$  and radii of  $\sim 1\text{--}7$  pc. Because of the high densities required to fit the data, we suggest that the less luminous of these sources are extragalactic ultracompact HII region complexes, those of intermediate luminosity are similar to W49 in the Galaxy, while the brightest will be counterparts to 30 Doradus when they emerge from their birth material. These objects constitute the lower mass range of extragalactic “ultradense HII regions” which we argue are the youngest stages of massive star cluster formation yet observed. The sample presented in this paper is beginning to fill in the continuum of objects between small associations of ultracompact HII regions and the analogous massive extragalactic clusters that may evolve into globular clusters.

*Subject headings:* galaxies: individual(M33, NGC 253, NGC 6946)—HII regions—galaxies: star clusters—radio continuum: galaxies

## 1. INTRODUCTION

In relatively nearby starburst galaxies, recent star formation activity has typically been resolved into massive star clusters. While old globular clusters are ubiquitous at the current epoch, only over the past decade have we begun to find their younger and bluer siblings, “super star clusters” (SSCs), in significant numbers (Whitmore 2000). The large number of globular clusters in the local universe appear to have been formed during the early stages of galaxy evolution. Therefore, studying the genesis of local SSCs can yield information about the environment in which globular clusters formed in the early universe. The conditions required for massive star cluster formation are far from understood, but it seems clear that extreme environments, uncommon in the local universe, are necessary. Current theories suggest that high pressures, such as those due to large-scale shocks in merging galaxies (Elmegreen & Efremov 1997), are required in order to form bound massive star clusters. In fact, there is a large body of evidence that globular clusters are formed in galactic interactions

and mergers (e.g., Whitmore 2000).

Recently, a handful of very young massive star clusters still embedded in their birth material have been discovered in the galaxies NGC 5253 (Turner, Ho, & Beck 1998), He 2-10 (Kobulnicky & Johnson 1999), NGC 2146 (Tarchi et al. 2000), and NGC 4214 (Beck, Turner, & Kovo 2000). Embedded in these heavily enshrouded clusters are hundreds of young massive stars that create surrounding H II regions and manifest themselves as optically thick free-free radio sources. Similar dense, inverted-spectrum H II regions exist around individual stars in our galaxy (i.e., ultracompact H II regions, UCH IIs, Wood & Churchwell 1989), albeit on a vastly smaller scale. Because of their apparent spectral similarity to galactic UCH IIs, Kobulnicky & Johnson (1999) dubbed these extragalactic objects “ultradense H II regions” (UDH IIs). The physical properties of these clusters are truly remarkable; the estimated sizes (a few parsecs), stellar masses (a few  $\times 10^{5-6} M_{\odot}$ ), ionizing luminosities ( $N_{\text{Ly}\alpha} \sim 10^{51-53}$  erg), and ages (possibly as young as a few  $\times 10^5$  years) of the newly discovered UDH IIs imply that we may be witnessing the birth process of super star clusters. The discovery of these UDH IIs allows us to begin observing the earliest stages of the massive star cluster formation for the first time.

Because UDH IIs have only recently been identified in the literature, one of our primary goals is simply to expand the sample of known objects in order to understand their properties in a statistical sense. To this end, we have searched for previously published radio observations that may have also serendipitously detected UDH IIs. Multiwavelength radio observations taken to study supernovae remnants in nearby galaxies are particularly useful for this purpose. In most cases, the original authors have identified the candidate UDH IIs we present here as “thermal sources” or “H II regions.” We seek sources with positive radio spectral indices ( $\alpha > 0$ , where  $S_{\nu} \propto \nu^{\alpha}$ ), implying an optically thick free-free origin. In this article, we utilize previously published radio observations of M33, NGC 253, and NGC 6946 to identify new candidate UDH IIs, determine their number of ionizing stars, and estimate their physical sizes, densities, and masses.

## 2. GALAXIES IN THIS SAMPLE

Here we overview basic properties of the galaxies in our sample and only highlight the radio observations utilized in this paper. We refer the reader to the original papers for more detail on the observations and reduction. Because the observations were compiled from a variety of sources, the observations are heterogeneous in nature, and in some cases, non-ideal for our purposes. For example, in order to obtain accurate relative fluxes at multiple frequencies it is desirable to have well matched beam sizes; we will discuss the impact of

mismatched beams in Section 3.1. However, these data provide a valuable resource for this fledgling field and will serve as a useful baseline for follow-up observations.

## 2.1. *M33*

M33 (NGC 598) is a Local Group spiral galaxy (Sc(s)II-III), nearly face-on ( $i = 55^\circ$ , Garcia-Gomez & Athanassoula 1991), and it is rich in H II regions (Hodge et al. 1999; Courtés et al. 1987; Boulesteix et al. 1974). Young ( $< 10^8$  yr) clusters in M33 were recently studied by Chandar et al. (1999), and were found to have masses of  $6 \times 10^2 - 2 \times 10^4 M_\odot$ , smaller than that typical for its old globular clusters. M33 has a star formation rate of  $\log(\text{SFR}) = -2.47 \text{ M}_\odot \text{ yr}^{-1} \text{ kpc}^{-2}$  (Kennicutt 1998), making it the least prolific galaxy in this sample. At a distance of 840 kpc (Freedman, Wilson, & Madore 1991), it is also the closest of the galaxies in this paper.

The radio observations of M33 that we use were originally obtained by Duric et al. (1993) and also presented by Gordon et al. (1999). Both Very Large Array (VLA) B configuration and Westerbork Synthesis Radio Telescope (WSRT) observations were made of M33 at 6 and 20 cm (4.84 and 1.42 GHz) in several pointings to obtain good coverage of the galaxy. The primary beams at 20 cm were  $30'$  with the VLA and  $36'$  with WSRT. At 6 cm both telescopes had primary beams of  $9'$ . The 6 cm observations had resolutions ranging from  $5''$  to  $10''$ , and the 20 cm observations had resolutions ranging from  $5''$  to  $15''$ , depending on the uv taper used in the cleaning process. Matched beam observations were convolved to identical beams of  $7''$  FWHM. All images have an average  $3\sigma$  rms noise level of  $\approx 150 \mu\text{Jy}$  per beam. At the adopted distance of 840 kpc (Freedman, Wilson, & Madore 1991),  $1 \text{ Jy} = 8.5 \times 10^{26} \text{ erg s}^{-1} \text{ Hz}^{-1}$ .

## 2.2. *NGC 253*

At 2.5 Mpc (Turner & Ho 1985), NGC 253 is a member of the Sculptor Group. This galaxy is a nearly edge-on spiral galaxy (Sc(s)), and contains a radio continuum plume emanating from the central starburst region rising perpendicular to the disk (e.g., Carilli et al. 1992). NGC 253 has the highest star formation rate of the galaxies in this sample with  $\log(\text{SFR}) = 1.24 \text{ M}_\odot \text{ yr}^{-1} \text{ kpc}^{-2}$  (Kennicutt 1998). Four young SSCs were discovered optically in the central region of NGC 253 by Watson et al. (1996); however, only one of these clusters is apparent in the mid-IR observations of Keto et al. (1999), who propose that it might be exceptionally young. Ulvestad & Antonucci (1997) also discuss the nature of the

brightest thermal radio source in NGC 253, a point that we will revisit in Section 3.

NGC 253 was observed by Ulvestad & Antonucci (1997) with the B configuration of the VLA at 1.3, 2, 3.6, 6, and 20 cm (23.56, 14.94, 8.44, 4.86, and 1.49 GHz) between 1987 and 1995. Additional observations at 1.3 and 2 cm were made using the A configuration. As the beam sizes at 6 and 20 cm are significantly larger than at 1.3, 2, and 3.6 cm, we have not included this longer wavelength data in our analysis because of the unwanted background contribution from non-thermal emission. The duration of the observations in the B-array were 4.1, 5.6, and 7.0 hours at 1.3, 2, and 3.6 cm, respectively. The A-array observations at 1.3 and 2 cm were 2.8 and 4.2 hours, respectively. The primary beams varied from 2' to 5' (from 1.3 cm to 3.6 cm, respectively) and easily contain the area of interest. The synthesized beams ranged from  $0.13'' \times 0.07''$  to  $0.42'' \times 0.24''$  at 1.3 cm,  $0.20'' \times 0.10''$  to  $0.59'' \times 0.35''$  at 2 cm, and  $0.33'' \times 0.19''$  to  $0.36'' \times 0.21''$  at 3.6 cm. Ulvestad & Antonucci (1997) estimate the uncertainties in these data as  $\sim 20\%$  for 1.3 cm, and  $\sim 10\%$  for the 2 cm and 3.6 cm data. The  $3\sigma$  rms noise levels are  $\approx 660$ , 240, and  $150 \mu\text{Jy}$ , respectively, for the 1.3 cm, 2 cm, and 3.6 cm data. At the adopted distance of 2.5 Mpc (Turner & Ho 1985),  $1 \text{ Jy} = 7.5 \times 10^{27} \text{ erg s}^{-1} \text{ Hz}^{-1}$ .

### 2.3. NGC 6946

NGC 6946 is the most distant galaxy in this sample at 5.1 Mpc<sup>1</sup> (de Vaucouleurs 1979), and is a spiral galaxy of type Sc(s)II with an inclination angle of  $i = 34^\circ$  (Garcia-Gomez & Athanassoula 1991). The star formation rate in NGC 6946 is  $\log(\text{SFR}) = -1.88 \text{ M}_\odot \text{ yr}^{-1} \text{ kpc}^{-2}$  (Kennicutt 1998). Larsen & Richtler (1999) have detected 107 young massive star clusters, one of which has received particular attention because of its age ( $\sim 15 \text{ Myr}$ ) and mass ( $\sim 5 \times 10^5 \text{ M}_\odot$ ) (Elmegreen, Efremov, & Larsen 2000). Sub-mm images obtained by Bianchi et al. (2000) show 850  $\mu\text{m}$  emission which, in some cases, may be associated with radio sources discussed in this paper.

The VLA was used to survey NGC 6946 with the B and A arrays at 6 and 20 cm (4.86 and 1.45 GHz), respectively, by Lacey, Duric, & Goss (1997). Approximately 8.6 hours were spent in at each frequency. The primary beams were 9' and 30' at 6 cm and 20 cm, respectively. The resulting beam sizes at the two wavelengths are very well matched:  $1''.9 \times 1''.6$  at 6 cm and  $1''.9 \times 1''.7$  at 20 cm. Flux uncertainties are typically  $\approx 20\%$ , and the  $3\sigma$  rms noise levels are  $\approx 60$  and  $50 \mu\text{Jy}$  for the 20 and 6 cm data, respectively. At the adopted distance of 5.1 Mpc (de Vaucouleurs, de Vaucouleurs, & Corwin 1976),  $1 \text{ Jy} = 3.1 \times 10^{28} \text{ erg s}^{-1} \text{ Hz}^{-1}$ .

---

<sup>1</sup>Distances as high as 10.1 Mpc have been estimated (e.g., Sandage & Tammann 1981).

These observations have also been analyzed by Hyman et al. (2000), who derive a luminosity function for H II region candidates with a power-law index at 6 cm of  $\approx -1.2$ , but exclude sources with spectral indices of  $\alpha > 0.2$ . As result, the most optically thick sources were excluded from their sample. Never the less, the seven sources presented in Hyman et al. (2000) with  $\alpha > 0$  are also included in this paper (our sources 1, 2, 4, 6, 7, 8, and 10 in Tables 3 and 6).

### 3. RESULTS

#### 3.1. Detection of UDHII Candidates

Our primary tool for distinguishing UDH IIs from other types of radio sources, such as supernovae remnants (SNR), is the radio spectral index  $\alpha$  (where  $S_\nu \propto \nu^\alpha$ ). While optically thin sources have  $\alpha = -0.1$ , optically thick sources have  $\alpha > -0.1$  ( $\alpha$  approaches 2 in the black body limit), and typical non-thermal objects have  $\alpha < -0.4$ . Unfortunately, not all SNRs obey this convention — in particular, there is a class of “composite” or “plerionic” SNRs (as coined by Weiler & Panagia 1978) that are known to have atypically flat spectral indices ( $-0.3 < \alpha < 0.0$ ). In fact, in the first few hundred days after a supernova explosion,  $\alpha$  can actually be positive (Weiler et al. 1986). However, given this extremely short timescale, we would have to be extremely fortunate (or unfortunate) to have one of these objects contained in our sample. A second set of observations taken with adequate time separation, such as those employed by Kobulnicky & Johnson (1999) would resolve this issue with confidence.

Consequently, in order to select UDH II candidates from the radio data, we have applied the condition that these sources must have radio spectral indices  $\alpha > 0$  (higher fluxes at shorter wavelengths). This criterion should exclude most other classes of radio-emitting objects, but it may also exclude genuine UDH II regions depending upon the exact instrumental angular resolution and frequencies observed. For example, low-frequency observations of optically thick thermal sources could be contaminated by steep-spectrum non-thermal sources, such as SNRs, and thus fail the  $\alpha > 0$  test, especially at longer wavelengths. Furthermore, more distant sources, or sources observed using beam sizes larger than the thermal emitting region, may be contaminated by steep-spectrum, non-thermal background emission that dominates the disks and halos of most galaxies. Both of these effects will act to disguise an optically thick thermal bremsstrahlung signature. Thermal sources with the lowest emission measure, and thus the lowest free-free optical depth will be affected most strongly. Sources with the highest emission measures are more likely to maintain a positive spectral signature and be correctly identified. Fortunately, it is precisely these sources with high emission

measures that are most likely to host ultra-young stellar clusters.

Because we are relying on relative fluxes at different frequencies to identify UDHIIs, it is critical that we understand the impact of beam sizes on these flux measurements. In some cases (as for NGC 6946), the multifrequency observations were done in different array configurations to match beam sizes at different frequencies. However, in some observations presented here the beam sizes are not well matched (as for M33). In these cases, typically a single configuration is used for all frequencies causing the beam size at the higher frequency to be smaller than the beam size at lower frequency. If the object (UDH II) is point-like with respect to the beams, the larger (lower frequency) beam will contain more non-thermal background contribution (as discussed above), which can only cause these objects to appear *less* thermal. If the object is extended, the lower frequency beam will contain more flux from the same physical environment than the higher frequency beam — again, artificially boosting the relative flux at the lower frequency, and also causing the object to appear *less* thermal. In other words, if the beam size at lower frequencies is larger than the beam size at higher frequencies (as is the case for the mis-matched beams in this paper), it will only disguise the optically thick signature of UDHIIs and *not* artificially imitate an optically thick thermal spectral index.

The condition that UDH II candidates must have positive spectral indices has resulted in the detection of fourteen sources in M33, five sources in NGC 253, and sixteen sources in NGC 6946. These sources are listed in Tables 1 – 3 along with their spectral indices ( $\alpha$ , where  $S_\nu \propto \nu^\alpha$ ). Within the uncertainties, eight of these objects are not inconsistent with having  $\alpha \lesssim 0$ , and we cannot rule out an optically thin H II region as the source. The remaining twenty-seven objects are only consistent with having an optically thick origin, and we consider these sources to be strong candidates for having an UCH II-like origin. Ulvestad & Antonucci (1997) have previously discussed the brightest of these five sources in NGC 253 (source #3 in this paper). Their derived properties ( $Q_{Lyc} = 5.2 \times 10^{51} \text{ s}^{-1}$ , size =  $2.4 \times 1.2 \text{ pc}$ ,  $EM = 2 \times 10^8 \text{ cm}^{-6} \text{ pc}$ , and  $n_e = 1.3 \times 10^4 \text{ cm}^{-3}$ ) are in excellent agreement with the values we derive for this object in this section. However, the properties of the other four sources were not discussed, and we wish to add these sources to the current sample of UDHIIs in the literature.

### 3.2. Comparison to Optical Images

As the gas and dust associated with UDHIIs dissipates and the extinction lessens, these objects will become more easily visible in optical light. On the other hand, UDHIIs will become less obvious in radio observations as their ambient densities decrease and their

thermal bremsstrahlung emission decreases as a result. *Consequently, optical surveys of HII regions will be biased against detecting the youngest HII regions and radio surveys will tend to miss the older HII regions.*

Therefore, in order to understand how these UDHII candidates are related to star formation, past or present, it is useful to examine optical images near the source positions. In most cases, this comparison reveals whether the UDHII regions are associated with star formation visible in optical light, diffuse HII emission, or are completely obscured in this wavelength regime. In making such comparisons in crowded fields, we must keep in mind that the radio positions are no better than about half a beam width, e.g.,  $3 - 4''$  in M33,  $1''$  in NGC 6946, and sub-arcsecond in NGC 253. To make these comparisons, we have tied the coordinate system of the optical images to the *HST* Guide Star “system.” This leads to small internal errors ( $0''.3$  RMS) within a galaxy, but it is well known that the same star will have coordinates that may differ by  $2''$  or more from plate to plate in the Guide Star Catalog. We thus expect systematic offsets between the optical and radio positions by as much as  $3''$ . This is possibly an overestimate, but we cannot rule out the physical correspondence of optical and radio sources within the astrometric uncertainty.

The locations of the UDHII regions in M33 were compared with B-band images from the 0.9 m telescope on Kitt Peak; see Massey et al. (1996) for a complete description of the observations. We also searched the catalogs of HII regions in M33 given by Boulesteix et al. (1974), Courtés et al. (1987), Hodge et al. (1999). M33 is rich in HII regions, and all of the UDHII regions are possibly associated with previously known HII regions, although in some cases the connection is insecure (Table 4). However, only about half of the UDHII regions appear to be associated with stellar light apparent in the B-band image. The locations of the detected UDHII regions with respect to the B-band image are shown in Figure 1.

The radio observations of NGC 253 were compared to archival F656N (narrow-band  $H\alpha$ ) and F814W (I-band) Hubble Space Telescope images (Figure 2). While there is diffuse emission in the vicinity of all five UDHII regions in this galaxy, only one of them (source #2) is clearly identified with a compact optical object. These results are presented in Table 5.

For NGC 6946, we compare the locations of the thermal radio sources with optical R-band and  $H\alpha$  images previously published by Larsen & Richtler (1999) (Figure 3). However, because of the large angular size of the galaxy ( $\sim 10' \times 10'$ ) this image does not have a wide enough field to contain all of the radio sources. Therefore, we also use images from the the STScI Digitized Sky Survey <sup>2</sup> for comparison in these cases (Figure 4). About half

---

<sup>2</sup>The compressed files of the Space Telescope Science Institute Quick-Survey of the northern sky are based on scans of plates obtained by the Palomar Observatory using the Oschin Schmidt Telescope.



of the sources in NGC 6946 have possible optical counterparts or diffuse emission, and the remaining half have neither.

While the sources for which there are no obvious optical counterparts must be deeply enshrouded, and therefore are likely to be extremely young, it isn't clear whether detection of light in the optical regime rules out extreme youth for UDH II regions. We make this tentative statement for several reasons: (1) in most cases presented in this sample, the identification of an optical counterpart is insecure due to the possible systematics between the optical and radio positions, as well as the relatively large synthesized radio beam-width for M33; (2) in cases where individual stars are resolved (M33), the *number* of stars required to create the Lyman continuum flux are not apparent in the optical images, suggesting either a misidentification due to pointing uncertainty, or a number of the individual stars are, in fact, still enshrouded. This scenario has actually been observed in the galactic UCH II complex W49A where *some* of the stars in the complex appear to have emerged from their birth cocoons while the rest of the complex remains enshrouded (Conti & Blum 2001) ; and (3) if the dominant source of opacity is Thompson scattering (and not dust), a source with a radius of 5 pc could have electron densities as high as  $n_e = 10^5 \text{ cm}^{-3}$  and still have opacities as low as  $\tau \sim 1$ . Therefore, we conclude that the possible identification of optical counterparts does not preclude the youth of these objects. However, the sources for which there are no optical counterparts are more likely deeply embedded in their natal molecular clouds, and therefore extremely young.

### 3.3. Modeled Properties

Given the luminosities and radio spectral energy distributions of H II regions, their physical parameters such as size and electron density can be estimated. Using the analytical approximation of Mezger & Henderson (1967), we can estimate the emission measure,  $EM = \int n_e^2 dl$ , given an electron temperature,  $T$ , the observing frequency,  $\nu$ , and the optical depth at that frequency.

$$EM(\text{cm}^{-6}\text{pc}) = 12.2 \left[ \frac{T_e}{(\text{K})} \right]^{1.35} \left[ \frac{\nu}{(\text{Ghz})} \right]^{2.1} \tau. \quad (1)$$

The positive spectral index for these sources arises from free-free emission where  $\tau \gtrsim 1$ , therefore we assume  $\tau = 1$  as a lower limit. The electron temperature of Galactic UCH IIs is typically  $T_e = 8000 \pm 1000 \text{ K}$  (e.g., Afflerbach et al. 1996), which we adopt for this estimate. The resulting emission measures for each of the wavelengths used in this sample range from  $\sim 0.05 - 16 \times 10^8 \text{ cm}^{-6} \text{ pc}$  (for  $\tau > 1$  these emission measures will be correspondingly higher).

Although the radio maps constrain the size of the emitting region only weakly <sup>3</sup>, it is clear that electron densities in excess of  $1000 \text{ cm}^{-3}$  are required to produce the observed emission measures. For comparison, typical giant H II regions observed optically have electron densities  $\approx 10^2 \text{ cm}^{-3}$  (Kennicutt 1984).

In order to better constrain the properties of the UDH II regions, following Kobulnicky & Johnson (1999) we have modeled H II regions as homogeneous spheres of plasma with uniform electron density and temperatures of 8000 K. Only free-free emission and absorption processes are considered. Varying the radius,  $R$ , and electron density,  $n_e$ , we modeled the radio spectral energy distribution resulting from thermal bremsstrahlung emission and self-absorption. These results are illustrated in Figures 5-7 along with the data from Tables 1–3. Figure 5 shows the 20 cm and 6 cm observations of UDH II regions in M33 along with two sets of model H II regions spectral energy distributions. Different symbols distinguish the UDH II candidates from Table 1. Solid lines show H II region models with electron densities of  $n_e = 5000 \text{ cm}^{-3}$  and radii of 0.7 pc and 1.9 pc. Although the modeled luminosities closely match the observed luminosities, the spectral index of these models is generally steeper than the data. A second class of models with electron densities of  $n_e = 1500 \text{ cm}^{-3}$  and radii of 1.5 pc to 3.0 pc more closely match the observed spectral indices and luminosities. In the case of NGC 6946, densities of  $1500 \text{ cm}^{-3}$  to  $5000 \text{ cm}^{-3}$  fit the 20 cm and 6 cm data for radii ranging from 2 pc to 7 pc (only a representative range of data from Table 3 are plotted). In the case of NGC 253, observations reveal that the UDH II regions are optically thick at frequencies as high as 15 GHz. Figure 6 illustrates that electron densities between  $10,000 \text{ cm}^{-3}$  and  $15,000 \text{ cm}^{-3}$  are required to fit the data. Not only are the UDH II regions in NGC 253 intrinsically more luminous than in the other two galaxies, they also have higher densities.

It is reasonable to ask whether the simple homogeneous sphere models presented here are sufficient to infer the physical characteristics (sizes, densities) of the UDH IIs. Realistically, we expect that the radio sources identified as UDH IIs are not simply monolithic dense H II regions. Rather, we expect that they are collections of several hundred ultra-compact H II regions ( $n_e = 10^5 \text{ cm}^{-3}$ ,  $R = 0.1 \text{ pc}$ ) embedded in a more tenuous inter-UCH II medium (see 4.2). However, two galaxies, NGC 253 (Ulvestad & Antonucci 1997) and NGC 5253 (Turner et al. 1999) are near enough and have observations with high enough resolution that the radio imaging can directly constrain the sizes of the emitting regions without recourse to model assumptions. In both cases, our simple homogeneous spherical models described above produce size estimates in excellent agreement with the high-resolution radio maps. The

---

<sup>3</sup>The radio maps constrain the sizes of the emitting regions to diameters  $\leq 4 \text{ pc}$  in the case of NGC 253,  $\leq 28 \text{ pc}$  in the case of M 33, and  $< 50 \text{ pc}$  in the case of NGC 6946

deconvolved diameters of the radio sources in NGC 253 are 2-4 pc, in excellent agreement with the best-fitting models shown in Figure 6. In NGC 5253, the single UDH II radio source has a deconvolved diameter of 1-2 pc (Turner, Beck, & Ho 2000), consistent with the expectations of the simple model predictions based on the observed radio luminosities of Turner et al. (1998). As further support for our simple models, recently Mohan, Anantharamaiah, & Goss (2001) have made slightly more sophisticated multi-density models for radio recombination line observations of He 2-10 and NGC 5253; their results are in excellent agreement with the results we find with our simple models.

Given the agreement in these two nearby cases, we believe that the simple two-parameter models are sufficiently instructive to make meaningful inferences about the sizes and densities of UDH IIs based on radio continuum luminosities. More realistic models would include an arbitrary number of UCH II regions within each UDH II each with its own density profile, and an inter-UCH II medium with a specified density profile and temperature distribution. However, relaxing the simple two-parameter approach results in the number of free parameters and computational complexity growing rapidly.

## 4. DISCUSSION

### 4.1. *Stellar Content*

The production rate of Lyman continuum photons, and, thus, the stellar content of each UDH II region can be estimated from the thermal radio luminosity following Condon (1992),

$$\left(\frac{Q_{Lyc}}{\text{s}^{-1}}\right) \geq 6.3 \times 10^{52} \left(\frac{T_e}{10^4 \text{K}}\right)^{-0.45} \left(\frac{\nu}{\text{GHz}}\right)^{0.1} \left(\frac{L_{thermal}}{10^{27} \text{erg s}^{-1} \text{Hz}^{-1}}\right). \quad (2)$$

Since the non-thermal component becomes weaker at higher frequencies, for each of the UDH IIs in this sample we use the luminosity measured at the highest frequency in each data set to determine  $Q_{Lyc}$ . The resulting values determined from this method are presented in Tables 1 – 3. One should also bear in mind that the  $Q_{Lyc}$  values determined with this method could suffer from two different problems: (1) if the source is, in fact, optically thick even at the highest frequencies measured, this method will *underestimate* the actual ionizing luminosity, and (2) if there is contamination from background non-thermal emission in the beam at the frequency used, the ionizing luminosity will be *overestimated*. While these two issues have an opposite affect on  $Q_{Lyc}$ , we can not determine the magnitude of either with the data presently available.

The production rate of Lyman continuum photons from these sources can be used to estimate the number of massive stars powering the observed emission. Following the convention

of Vacca (1994), a “typical” O-star (type O7V) produces  $Q_{Ly\alpha} = 1.0 \times 10^{49} \text{ s}^{-1}$ . Therefore, the  $Q_{Ly\alpha}$  values in Tables 1-3 can be directly translated into the number of “equivalent” O7V stars (O7V\*). Using this method, we see that the UDH II regions in this sample have  $\approx 3-46$  O7V\* stars in M33,  $\approx 60 - 560$  in NGC 253, and  $\approx 10 - 360$  in NGC 6946. Moreover, the *total* stellar mass of these objects can be estimated using the Starburst99 models of Leitherer et al. (1999) with solar metallicity, Salpeter IMF, and lower and upper mass cutoffs of  $1M_{\odot}$  and  $100M_{\odot}$ , respectively (decreasing the lower mass limit will increase the total stellar mass estimate). Using these parameters, star clusters producing this range of Lyman continuum photons at ages  $\sim 0 - 5$  Myr would have total masses of  $\sim 100 - 60000M_{\odot}$ .

These  $Q_{Ly\alpha}$  and mass values are smaller than those found for the UDH IIs in NGC 5253 (Turner, Ho, & Beck 1998), Henize 2-10 (Kobulnicky & Johnson 1999), and NGC 2146 (Tarchi et al. 2000), which have  $> 750$  O7V\* stars and masses  $> 10^5 M_{\odot}$ . This is not a surprising result – it is likely that we will only find massive star clusters forming in intense starburst events; Elmegreen & Efremov (1997) have demonstrated the need for extremely high-pressure environments, such as those found in starburst galaxies, to produce bound massive star clusters. However, in less formidable environments, we should expect to find a continuous range of UDH IIs — from single UCH IIs and UCH II complexes (such as those found in the Galaxy), to the massive bound clusters (such as those found in NGC 5253, Henize 2-10, and NGC 2146) that may evolve into globular clusters. The sample presented in this article is beginning to fill in this continuum of objects.

#### 4.2. Comparison to W49A

One of the most well studied UCH II complexes in the Galaxy is W49A, which makes it well suited for comparison to the UDH II regions in this sample. First detected by Westerhout (1958) in his radio survey, W49A has since been resolved into at least 30 UCH II regions (DePree, Mehringer, & Goss 1997), and is estimated to have  $\sim 100$  O7V\* stars (Smith, Biermann, & Mezger 1978; Vacca 1994). It also appear that a few of the stars in W49A have begun to emerge from their birth cocoons while the rest of the cluster remains deeply enshrouded (Conti & Blum 2001). W49A is  $\sim 13$  pc in diameter (DePree, Mehringer, & Goss 1997), and would fit within the beam sizes utilized in this paper if located at the same distances as the galaxies in this sample; W49A would have angular sizes of  $\sim 2''.9$ ,  $1''.2$ , and  $0''.6$ , respectively, in M33, NGC 253, and NGC 6946. Because W49A is significantly closer ( $D = 11.4$  kpc; Gwinn, Moran, & Reid 1992), than the galaxies presented in this paper, any observations we use for comparison need to be at sufficiently low resolution as to include the entire W49A region. This condition is well-satisfied by the pioneering observations of

Mezger, Schraml, & Terzian (1967), who obtained  $\sim 3 - 4'$  resolution radio maps of W49A at several wavelengths.

In Figure 8, we present the radio spectral energy distribution of W49A (Mezger, Schraml, & Terzian 1967) in comparison to the *mean* UDHII region from M33, NGC 253, and NGC 6946. It is clear that the integrated radio spectral energy distribution of W49A is almost identical to those of the UDHII regions in this sample. Figure 9 shows histograms of the 6 cm luminosities for the sources in M33 and NGC 6946 and the 3.6 cm luminosities (6 cm data is not included in this sample) for NGC 253 along with an arrow indicating the luminosity of W49A. Comparing the luminosity of W49A to those of the UDHII regions in M33, it is clear that W49A is up to 10 times *more* luminous than the M33 sources. In NGC 6946 W49A would be one of the more luminous HII regions. However, in the case of NGC 253, W49A would be one of the *least* luminous objects — a magnitude or more fainter than the most luminous UDHII regions detected in this galaxy.

The dotted line in Figure 9a illustrates the luminosity function of optically selected HII regions in M33 (Smith & Kennicutt 1989) who find  $N(L) \propto L^{-2.3} dL$ . This comparison shows that the luminosity function of UDHII regions is consistent with the normal HII region luminosity function, suggesting that the UDHII regions are simply a phase in the formation of many, perhaps most, HII regions. Furthermore, if the formation of massive star clusters is primarily related to the intensity of the star formation a galaxy is currently undergoing, it is not surprising that the UDHII regions in M33 and NGC 6946 are similar to the UCHII complexes in the Milky Way which has a similar star formation rate. NGC 253, by contrast, has a much higher star formation rate based on its FIR luminosity, although high visual extinctions make the  $H\alpha$  luminosities very uncertain. It certainly contains a more intense starburst, which is also in accord with the more massive UDHII regions it hosts.

#### 4.3. *On the Youth of UDHII Regions*

It seems likely that the fraction of time a super star cluster spends in the UDHII phase is a small fraction of the massive star lifetime, perhaps 10-15%, in accord with the estimated lifetimes of individual UCHII regions based on the number of UCHII regions compared with the number of optically visible O stars in the Galaxy (e.g., Wood & Churchwell 1989b). Indeed, UCHII region lifetimes have been a topic of much discussion since Wood & Churchwell (1989a) introduced the “lifetime problem”; in short, if UCHII regions are significantly overpressured with respect to the surrounding ISM, they should expand and dissipate on time scales  $\approx 10^4$  years. However, the number of UCHII regions observed is greater than is allowed for by this time scale. Several mechanisms have been proposed to address this

issue, most of which are likely to also be applicable to UDH IIs. Wood & Churchwell (1989a) proposed that infalling matter or bow shocks might act to increase the external pressure, thus extending the UCH II phase. It is also possible that the ambient pressure is typically significantly higher than the value used by Wood & Churchwell (1989a) as proposed by DePree, Rodríguez, & Goss (1995). The lifetimes of UCH II regions could also be extended if they are replenished by material photoevaporated from the surrounding circumstellar disks (e.g., Hollenbach et al. 1994).

The first argument for the extreme youth of UDH II regions is simply by analogy to UCH II regions in the Galaxy. If UDH IIs are composed of individual UCH II regions, we should expect them to have similar lifetimes provided that star formation is relatively instantaneous over the massive star cluster. As is the case for UCH II regions, the densities in UDH IIs are extremely high, and the implied pressures constitute an over-pressure compared to typical ISM pressures. To first order, such over-pressed regions must expand and disperse on time scales comparable to the sound-crossing time scale which is a few  $\times 10^5$  yr (see Kobulnicky & Johnson 1999 for more complete details). However, as discussed above for UCH II regions, it is entirely possible that the ambient pressure around UDH IIs is not “typical” of the global ISM.

The second piece of evidence suggesting extreme youth is the fraction of ionizing stars in UDH II regions compared to the fraction of ionizing stars in conventional H II regions. For M33 and NGC 6946 the minimum implied total Lyman continuum photon production rate,  $Q$ , of the UDH II regions is  $1.9 \times 10^{51} \text{ s}^{-1}$  and  $10 \times 10^{51} \text{ s}^{-1}$  respectively (provided there is no leakage from the enshrouding cocoon that would likely result in associated  $H\alpha$  emission). The total  $Q$  for the entire galaxy is  $3 \times 10^{53} \text{ s}^{-1}$  for M33 and  $1.5 \times 10^{53} \text{ s}^{-1}$  for NGC 6946 (Kennicutt 1983 scaled to our adopted distance). Thus, the UDH II regions contain 1% and 7% of the total ionizing photons. If the star formation has been reasonably continuous in these systems, a plausible estimate for the typical duration of the UDH II phase is 0.01 and 0.07 times the typical H II region lifetime ( $\times 10^7$  yr). This implies a mean age of less than 1 Myr for UDH II regions.

The third, and perhaps weakest, piece of evidence in favor of the extreme youth of UDH II regions comes from their high visual extinctions. In this article, we note that many of the ionizing star clusters within the UDH II regions are not visible at optical wavelengths. In some cases, only diffuse  $H\alpha$  emission is seen. Sams et al. (1994) show that in NGC 253, the extinctions due to dust reach local maxima, as high as  $A_V = 15$  mag at the positions of the radio sources we have identified as UDH II regions. This picture is consistent with UDH IIs being extremely young H II regions still hidden from view by the dust associated with their natal molecular clouds. However, one must also bear in mind that we cannot

rule out screens of dust not physically associated with the regions of optically thick free-free emission.

#### 4.4. *Future Work*

We expect that deliberate radio continuum searches will continue to find UDH II regions in all galaxies with sufficiently high levels of recent star formation. It is becoming clear that we are seeing a *continuum* of sizes and luminosities for extragalactic massive star clusters in the earliest stages of their evolution. We predict that the natal cocoons of UDH II regions should be prodigious emitters in the mid- to far-infrared regimes. In fact, mid- to far-infrared observations will allow us to search for an *even earlier* stage of massive star cluster evolution; before the stars have begun ionizing their surrounding ISM, they should go through a “hot core” phase, analogous to individual massive stars in the Galaxy. This phase will be defined by extremely dense and warm gas that is not associated with strong free-free emission. Therefore, further study of these sources will be greatly enhanced by upcoming mid- to far-infrared telescope missions, such as the Space Infrared Telescope Facility (SIRTF). Recognition of the ubiquity of the UDH II phase of massive star formation pushes one step closer to understanding the genesis mechanisms of all star clusters, from small associations to giant proto-globular clusters.

It is a delight to thank Paul Crowther, Dick McCray, and Sara Beck for useful discussions on this subject. Ed Churchwell provided useful feedback on a draft of this paper, for which we are grateful. The comments from the anonymous referee led to many improvements in the manuscript. We also extend our appreciation to Soeren Larsen for the use of his optical images in this study. The Digitized Sky Surveys were produced at the Space Telescope Science Institute under U.S. Government grant NAG W-2166. The images of these surveys are based on photographic data obtained using the Oschin Schmidt Telescope on Palomar Mountain and the UK Schmidt Telescope. The plates were processed into the present compressed digital form with the permission of these institutions. K.E.J. is pleased to acknowledge support for this work provided by NASA through a Graduate Student Researchers Fellowship. P.S.C. appreciates continuous support from the National Science Foundation.

## REFERENCES

- Afflerbach, A., Churchwell, E., Acord, J.M., Hofner, P., Kurtz, S., & Depree, C.G. 1996, ApJS, 106, 423

- Beck, S.C., Turner, J.L., & Kovo, O. 2000, *AJ*, 120, 244
- Bianchi, S., Davies, J.I., Alton, P.B., Gerin, M. & Casoli, F. 2000, *A&A*, 353, L13
- Boulesteix, J., Courtes, G., Laval, A., Monnet, G., & Petit, H. 1974, *A&A*, 37, 33
- Carilli, C.L., Holdaway, M.A., Ho, P.T.P., & de Pree, C.G. 1992, *ApJ*, 399, L59
- Chandar, R., Bianchi, L., Ford, H.C., & Salasnich, B. 1999, *PASP*, 111, 794
- Condon, J. J. 1992, *ARA&A*, 30, 575
- Conti, P.S. & Blum, R. 2001, in preparation
- Courtés, G., Petit, H., Petit, M., Sivan, J.-P., & Dodonov, S. 1987, *A&A*, 174, 28
- DePree, C.G., Rodríguez, L.F., & Goss, W.M. 1995, *RMxAA*, 31, 39.
- DePree, C.G., Mehringer, D.M., & Goss 1997, *ApJ*, 482, 307
- de Vaucouleurs, G. 1979, *ApJ*, 227, 729
- de Vaucouleurs, G., de Vaucouleurs, A., Corwin, H.G., Jr. 1976, *Second Reference Catalogue of Bright Galaxies* (2d ed.; Austin, TX: Univ. Texas Press)
- Duric, N., Viallefond, F., Goss, W.M., & van der Hulst, J.M. 1993, *A&AS*, 99, 217
- Elmegreen, B.G. & Efremov, Y.N. 1997, *ApJ*, 480, 235
- Elmegreen, B.G., Efremov, Y.N., & Larsen, S. 2000, *ApJ*, 535, 748
- Freedman, W.L., Wilson, C.D., & Madore, B.F. 1991, *ApJ*, 372, 455
- Garcia-Gomez, C. & Athanassoula, E. 1991, *A&AS*, 89, 159
- Gordon, S.M., Duric, N., Kirshner, R.P., Goss, W.M., & Viallefond, F. 1999, *ApJS*, 120, 247
- Gwinn, C.R., Moran, J.M., & Reid, M.J. 1992, *ApJ*, 292, 149
- Hyman, S.D., Lacey, C.K., Weiler, K.W., & Van Dyk, S.D. 2000, *AJ*, 119, 1711
- Hodge, P.W., Balsley, J., Wyder, T.K., & Skelton, B.P. 1999, *PASP*, 111, 685
- Hollenbach, D., Johnstone, D., Lizano, S., & Shu, F. 1994, *ApJ*, 428, 654
- Kennicutt, R.C., Jr. 1983, *ApJ*, 272, 54



- Kennicutt, R.C., Jr. 1984, ApJ, 287, 116
- Kennicutt, R.C., Jr. 1998, ApJ, 498, 541
- Keto, E., Hora, J.L., Fazio, G.G., Hoffmann, W., & Deutsch, L. 1999, ApJ, 518, 183
- Kobulnicky, H.A. & Johnson, K.E. 1999, ApJ, 527, 154
- Lacey, C., Duric, N., Goss, W.M. 1997, ApJS, 109, 417
- Larsen, S. S. & Richtler, T. 1999, A&A, 345, 59
- Leitherer, C. et al. 1999, ApJS, 123, 3
- Massey, P., Bianchi, L., Hutchings, J.B., & Stecher, T.P. 1996, ApJ, 469, 629
- Mezger, P.G., Schraml, J., & Terzian, Y. 1967, ApJ, 150, 807
- Mezger, P.G. & Henderson, A.P. 1967, ApJ, 147, 471
- Mohan, N.R., Anantharamaiah, K.R., & Goss, W.M. 2001, ApJ in press
- Sams, B. J. III, Genzel, R., Eckart, A., Tacconi-Garman, L., & Hoffman, R. 1994, ApJ, 430, L33
- Sandage, A. & Tammann, G.A. 1981, A Revised Shapley-Ames Catalog of Bright Galaxies (Carnegie Inst. Washington Publ. 635)(Washington: Carnegie Inst. Washington)
- Smith, T.R. & Kennicutt, R.C., Jr. 1989, PASP, 101, 649
- Smith, L.F., Biermann, P., & Mezger, P.G. 1978, A&A, 66, 65
- Tarchi, A., Neininger, N., Greve, A., Klein, U., Garrington, S.T., Muxlow, T.W.B., Pedlar, A., & Glendenning, B.E. 2000, A&A, 358,95
- Turner, J.L. & Ho, P.T.P. 1985, ApJ, 299, L77
- Turner, J.L., Beck, S.C., & Ho, P.T.P. 1998, ApJ, 532, L109
- Turner, J.L., Beck, S.C., & Ho, P.T.P. 2000, ApJL, 532, 109
- Ulvestad, J.S. & Antonucci, R.R.J. 1997, ApJ, 488, 621
- Vacca, W.D. 1994, ApJ, 421, 140

- Watson, A.M., Gallagher, J.S., III, Holtzman, J.A., Hester, J.J., Mould, J.R., Ballester, G.E., Burrows, C.J., Casertano, S., Clarke, J.T., Crisp, D., Evans, R., Griffiths, R.E., Hoessel, J.G., Scowen, P.A., Stapelfeldt, K.R., Trauger, J.T., & Westphal, J.A. 1996, AJ, 112, 534
- Weiler, K.W. & Panagia, N. 1978, A&A, 70, 419
- Weiler, K.W., Sramek, R.A., Panagia, N., van der Hulst, J.M., & Salvati, M. 1986, ApJ, 301, 790
- Westerhout, G. 1958, Bull. Ast. Inst. Netherlands, 14, 215
- Whitmore, B. 2000, in: Celebrating 10 Years of HST Symposium, May 2000, in press
- Wood, D.O. & Churchwell, E. 1989a, ApJS, 69, 831
- Wood, D.O. & Churchwell, E. 1989b, ApJ, 340, 265

Table 1. UDH II candidates in M33

#	R.A.	Dec.	$L_6$ $\times 10^{23}$	$L_{20}$ $\times 10^{23}$	$Q_{Lyc}$ $\times 10^{49}$	$\alpha_6^{20}$
	(2000)	(2000)	<i>erg/s/Hz</i>	<i>erg/s/Hz</i>	$s^{-1}$	
1	1:33:02.4	30:46:42.9	11.9±0.8	6.8±1.7	9.7±0.9	0.46±0.11
2	1:33:16.0	30:56:45.9	16.9±1.7	14.4±2.5	13.9±1.6	0.13±0.09
3	1:33:16.5	30:52:50.3	55.9±1.7	35.6± 2.5	45.8±1.4	0.37±0.03
4	1:33:37.5	30:47:19.3	9.3±0.8	7.6±0.8	7.6±6.2	0.17±0.06
5	1:33:39.2	30:38:06.9	9.3±0.8	7.6±1.7	7.6±6.2	0.17±0.10
6	1:33:43.6	30:39:07.1	8.5±0.8	7.6±1.7	6.9±0.8	0.09±0.10
7	1:33:48.2	30:39:17.8	3.4±0.8	2.5±0.8	2.8±0.7	0.25±0.17
8	1:33:59.8	30:32:45.3	3.4±0.8	2.5±0.8	2.8±0.7	0.25±0.17
9	1:34:00.2	30:40:47.7	46.6±0.8	42.4±1.7	38.2±2.2	0.08±0.02
10	1:34:02.2	30:38:40.7	28.8±2.5	26.3±2.5	23.6±2.5	0.07±0.06
11	1:34:06.4	30:41:45.6	11.±0.8	7.6±0.8	9.0±0.9	0.30±0.06
12	1:34:13.7	30:34:51.4	11.±0.8	7.6±0.8	9.0±0.9	0.30±0.06
13	1:34:17.3	30:33:43.4	7.6±0.8	6.8±0.8	6.2±0.8	0.09±0.07
14	1:34:38.9	30:43:59.7	7.6±0.8	5.9±1.7	6.2±0.8	0.21±0.13

<sup>a</sup>These coordinates are accurate to approximately the half beam width of  $\approx 3 - 4''$ .

Table 2. UDH II candidates in NGC 253

#	R.A.	Dec.	$L_{1.3}$ $\times 10^{24}$	$L_2$ $\times 10^{24}$	$L_{3.6}$ $\times 10^{24}$	$Q_{Lyc}$ $\times 10^{49}$	$\alpha_{1.3}^{3.6}$
	(2000)	(2000)	<i>erg/s/Hz</i>	<i>erg/s/Hz</i>	<i>erg/s/Hz</i>	$10^{49} s^{-1}$	
1	0:47:32.75	-25:17:20.94	6.3±1.3	—	5.±0.5	60±13	0.19±0.10
2	0:47:32.85	-25:17:20.34	33.6±6.7	25.6±2.6	20.5±2.0	319±66	0.41±0.10
3	0:47:33.05	-25:17:18.25	59.1±11.8	58.6±5.9	49.0±4.9	561±120	0.15±0.10
4	0:47:33.05	-25:17:17.65	20.6±4.1	—	18.1±1.8	196±41	0.11±0.10
5	0:47:33.25	-25:17:15.55	50.4±10.1	44.2±4.4	29.7±3.	479±100	0.43±0.10

<sup>a</sup>These coordinates are accurate to approximately the half beam width of  $\approx 0.1 - 0.2''$ .

Table 3. UDH II candidates in NGC 6946

#	R.A.	Dec.	$L_6$ $\times 10^{24}$	$L_{20}$ $\times 10^{24}$	$Q_{Ly\alpha}$ $\times 10^{49}$	$\alpha_6^{20}$
	(2000)	(2000)	<i>erg/s/Hz</i>	<i>erg/s/Hz</i>	<i>s</i> <sup>-1</sup>	
1	20:34:19.79	60:10:06.46	11.3±1.9	10.4±1.3	92.7±16	0.07±0.09
2	20:34:22.58	60:10:34.12	43.6±1.9	33.9±2.2	358.0±26	0.21±0.03
3	20:34:32.35	60:10:12.48	3.8±0.9	1.3±0.9*	30.9±7.9	0.88±0.32
4	20:34:33.89	60:11:25.07	4.7±1.3	3.8±0.9	38.6±11	0.17±0.16
5	20:34:39.70	60:08:22.79	6.0±0.6	1.9±0.6*	49.05±.8	0.94±0.14
6	20:34:49.38	60:08:00.64	4.1±0.6	3.1±0.9	33.5±5.5	0.23±0.14
7	20:34:54.25	60:08:53.62	5.6±1.3	5.3±0.9	46.3±11	0.05±0.13
8	20:34:54.52	60:07:39.73	8.8±0.9	8.2±0.9	72.1±8.7	0.06±0.07
9	20:34:56.49	60:08:20.25	2.5±0.6	1.9±0.9*	20.6±5.3	0.23±0.23
10	20:35:03.67	60:10:59.66	3.4±0.9	3.1±1.3	28.3±7.9	0.08±0.22
11	20:35:04.35	60:09:46.09	3.8±1.3	2.2±1.3*	30.9±10	0.45±0.30
12	20:35:05.08	60:10:57.44	1.3±0.9*	0.9±0.6*	10.3±7.7	0.30±0.42
13	20:35:13.95	60:08:52.14	6.6±1.3	4.1±0.9	54.0±11	0.39±0.13
14	20:35:18.06	60:09:06.17	10.4±1.3	6.6±1.9	85.3±11	0.37±0.14
15	20:35:22.09	60:07:22.90	5.3±1.3	3.80±.9	43.8±11	0.27±0.15
16	20:35:24.12	60:08:42.61	3.8±0.9	2.2±0.6*	30.9±7.9	0.45±0.15

\*These luminosities represent less than a  $4\sigma$  detection.

<sup>a</sup>These coordinates are accurate to approximately the half beam width of  $\approx 1''$ .

Table 4. Comparison with optical images of M33

Source #	B-band Counterpart?	H II Counterpart?	GDKG #
1	point source offset?	HBW 193 ?	15
2	diffuse, point source offset?	BCLMP 638	33
3	diffuse, point source	BCLMP 623	34
4	no	BCLMP 611 ?	67
5	diffuse emission	BCLMP 35/36	71
6	diffuse emission	BCLMP 39/40	82
7	no, dust lane?	BCLMP 43 ?	91
8	diffuse emission	BCLMP 703 ?	128
9	no, dust lane?	Z 171/179	129
10	diffuse emission offset?	BCLMP 87	137
11	point source	BCLMP 77	142
12	point source offset?	BCLMP 714	151
13	diffuse emission	BCLMP 712	161
14	complex source	BCLMP 749/750	178

<sup>a</sup>HBW refers to the Hodge et al. (1999) catalog.

<sup>b</sup>BCLMP refers to the Boulesteix et al. (1974) catalog.

<sup>c</sup>Z refers to the Courtés et al. (1987) catalog.

<sup>d</sup>GDKG refers to the reference number in Gordon et al. (1999).

Table 5. Comparison with optical images of NGC 253

Source #	I-band Counterpart?	H $\alpha$ Counterpart?	UV #
1	complex source	complex source	5.45-42.8
2	complex source	complex source	5.54-42.2
3	complex source?	diffuse emission?	5.72-40.1
4	complex source?	diffuse emission?	5.73-39.5
5	diffuse emission?	diffuse emission	5.90-37.4

<sup>a</sup>UV # refers to the reference number in Ulvestad & Antonucci (1997).

Table 6. Comparison with optical images of NGC 6946

Source #	R-band Counterpart?	H $\alpha$ Counterpart?	LDG #
1	diffuse emission	—	3
2	no	—	5
3	diffuse emission	faint source?	10
4	diffuse emission	diffuse emission	11
5	no	no	24
6	point source	point source	42
7	no	no	73
8	complex source	complex source	76
9	no	no	79
10	no	no	87
11	no	no	90
12	diffuse emission	diffuse emission	94
13	diffuse emission	diffuse emission	109
14	diffuse emission	—	111
15	no	—	113
16	no	—	116

<sup>a</sup>LDG # refers to the reference number in Lacey, Duric, & Goss (1997).



Fig. 1.— Locations of the detected UDH IIs in M33 are shown (along with their number in Table 1) with respect to the B-band images (shown in gray scale). The identification circles are  $\sim 7''$  in diameter, reflecting the beam size of the radio observations. North is up and East is left. These images are all approximately  $1'.5$  on a side.

Fig. 2.— Locations of the detected UDH IIs in NGC 253 are shown (along with their number in Table 2) with respect to the  $H\alpha$  image (left) and I-band image (right). The identification circles are  $\sim 2''$  in diameter, reflecting the astrometric precision of *HST*. North is up and East is left. The  $H\alpha$  image is approximately  $12''.7 \times 12''.7$ , and the I-band image is approximately  $11''.6 \times 11''.6$ .

Fig. 3.— Locations of the detected UDH IIs candidates #3–12 in NGC 6946 are shown (along with their number in Table 3) with respect to the  $H\alpha$  (left) and R-band (right) images of Larsen & Richtler (1999). The identification circles are  $\sim 3''$  in radius, reflecting the relative astrometric uncertainty. North is up and East is left. These images are approximately  $1'.6 \times 1'.6$ .

Fig. 4.— Locations of the detected UDH IIs are shown (along with their number in Table 3) with respect to the Digitized Sky Survey (sources 1–2 and 13–16). The identification circles are  $\sim 3''$  in radius, reflecting the relative astrometric uncertainty. North is up and East is left. These Digitized Sky Survey images are approximately  $3'.6 \times 3'.6$ .

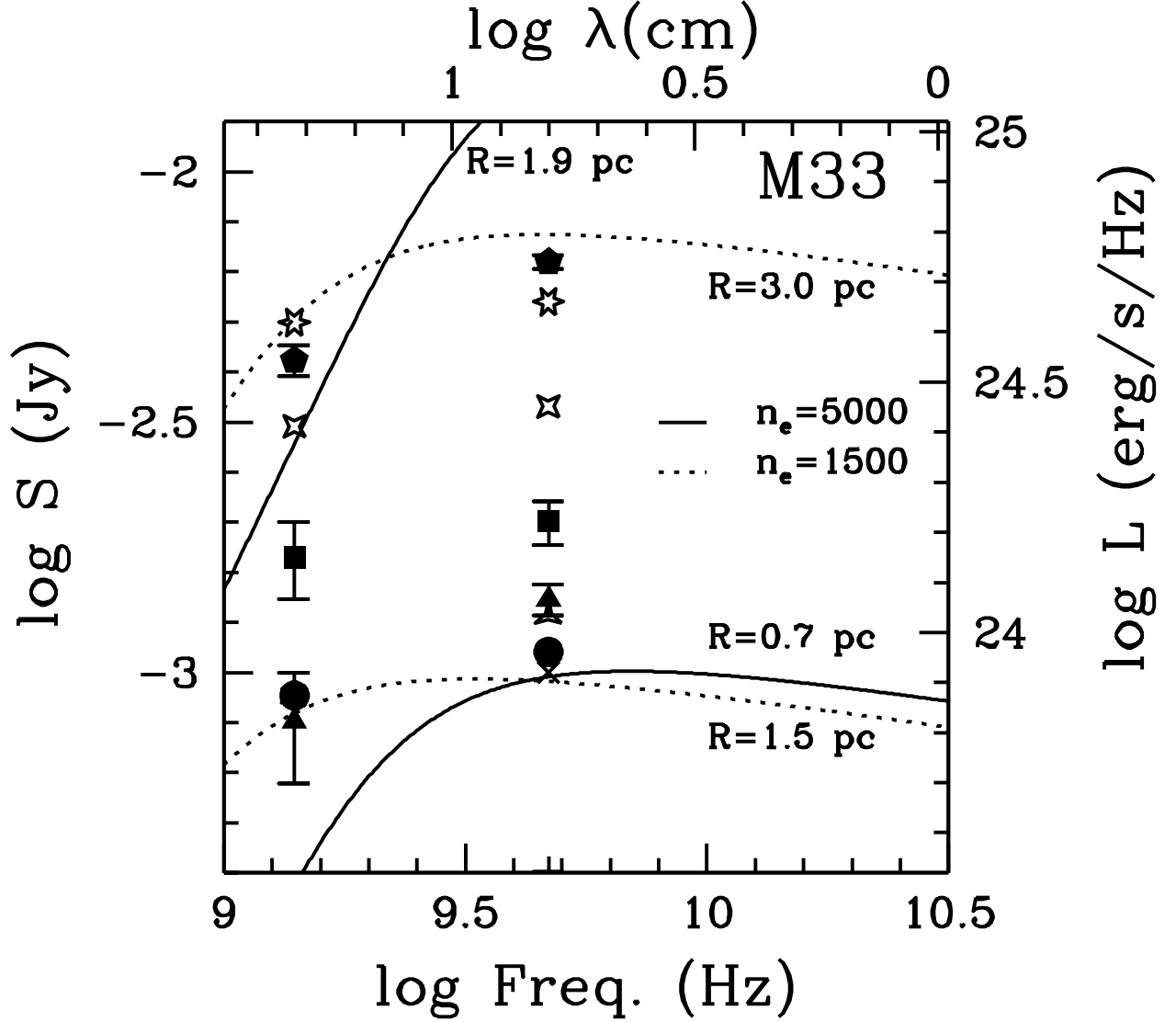


Fig. 5.— The radio fluxes and luminosities for the brightest UDHII candidates in M33 from Table 1. A different symbol is used for each source. A typical range of uncertainties is indicated, and we refer the reader to Table 1 for the remaining values. The radio data are consistent with model HII regions (solid and dashed lines) having electron densities  $n_e = 1500 - 5000 \text{ cm}^{-3}$  and radii  $R = 0.7 - 3 \text{ pc}$ .

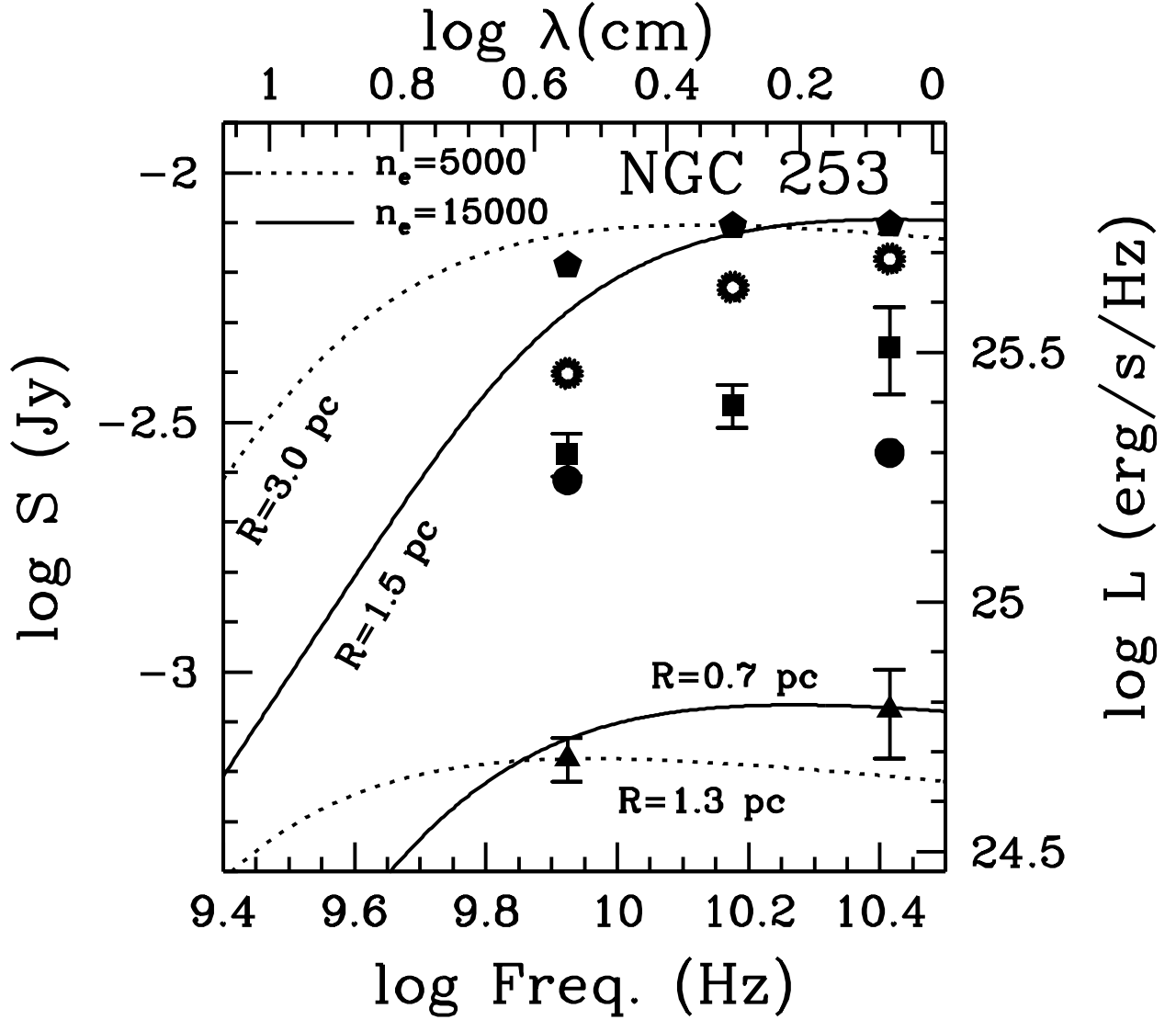


Fig. 6.— The radio fluxes and luminosities for the UDH IIs candidates in NGC 253. A different symbol is used for each source in Table 2. A typical range of uncertainties is indicated, and we refer the reader to Table 2 for the remaining values. The radio data imply high free-free optical depths at frequencies as high as 15 GHz. The data are consistent with model H II regions (solid and dashed lines) having electron densities  $n_e = 5000 - 15000 \text{ cm}^{-3}$  and radii  $R = 0.4 - 2 \text{ pc}$ .

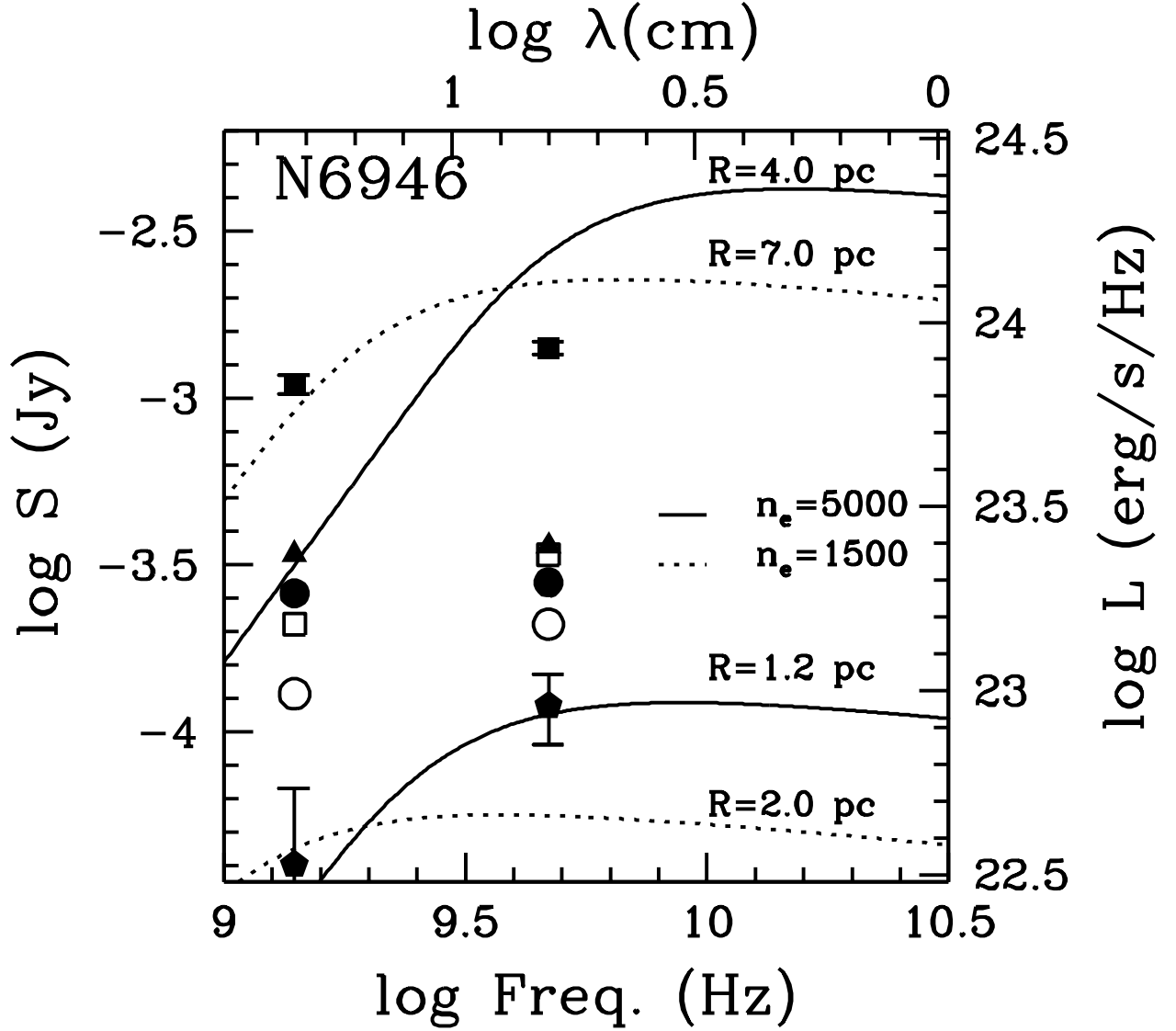


Fig. 7.— The radio fluxes and luminosities for the brightest UDH IIs candidates in NGC 6946 in Table 3. A different symbol is used for each source. A typical range of uncertainties is indicated, and we refer the reader to Table 3 for the remaining values. The data are consistent with model HII regions (solid and dashed lines) having electron densities  $n_e = 1500 - 5000 \text{ cm}^{-3}$  and radii  $R = 2 - 7 \text{ pc}$ .

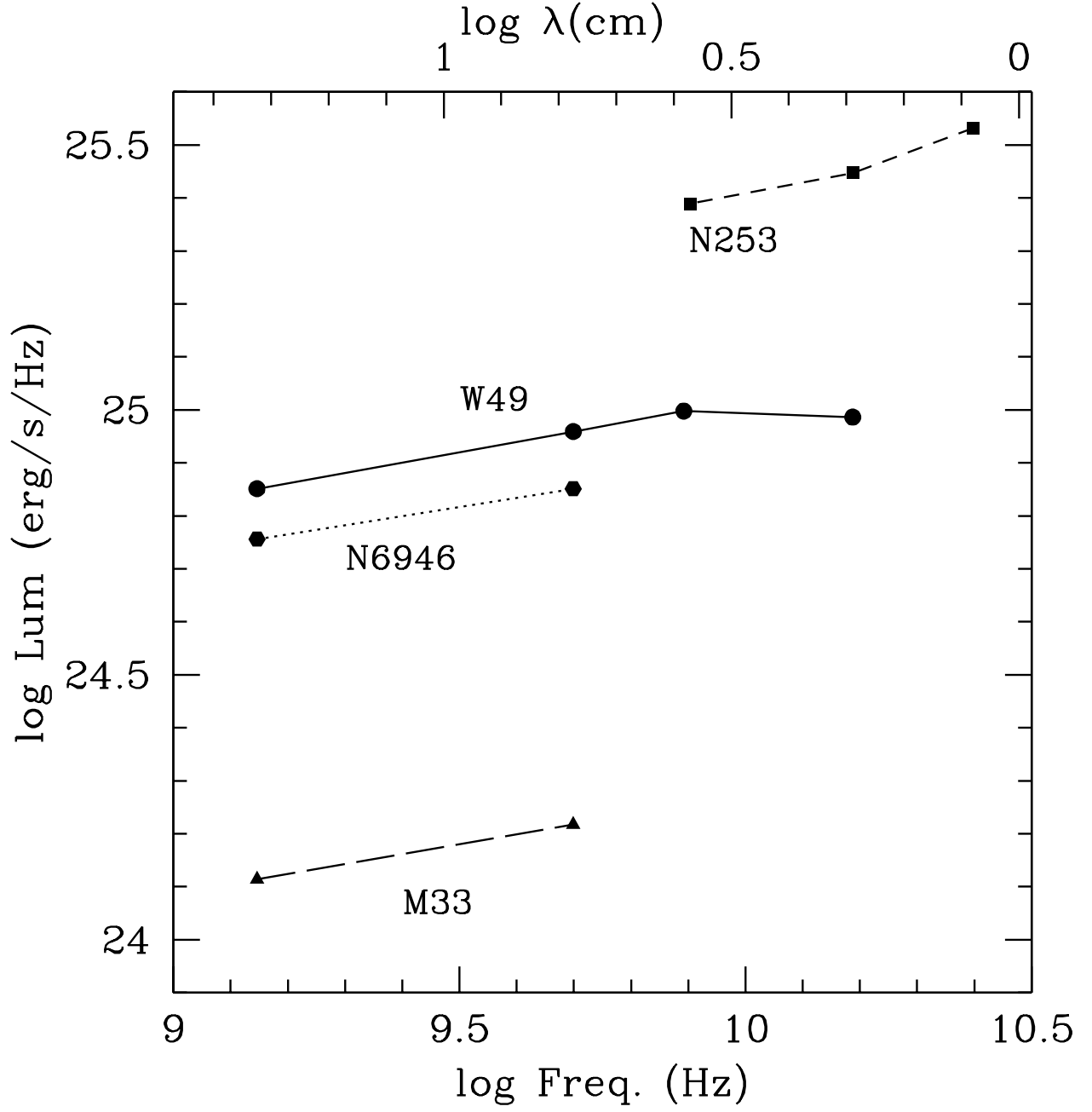
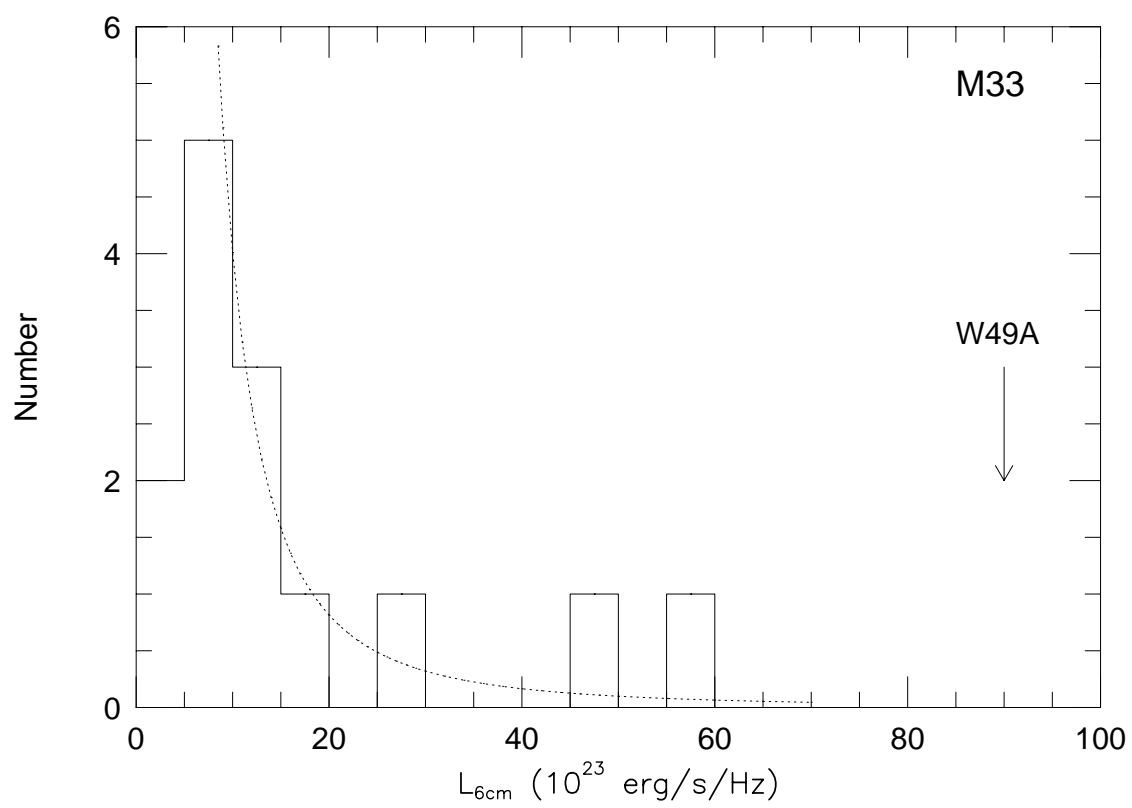
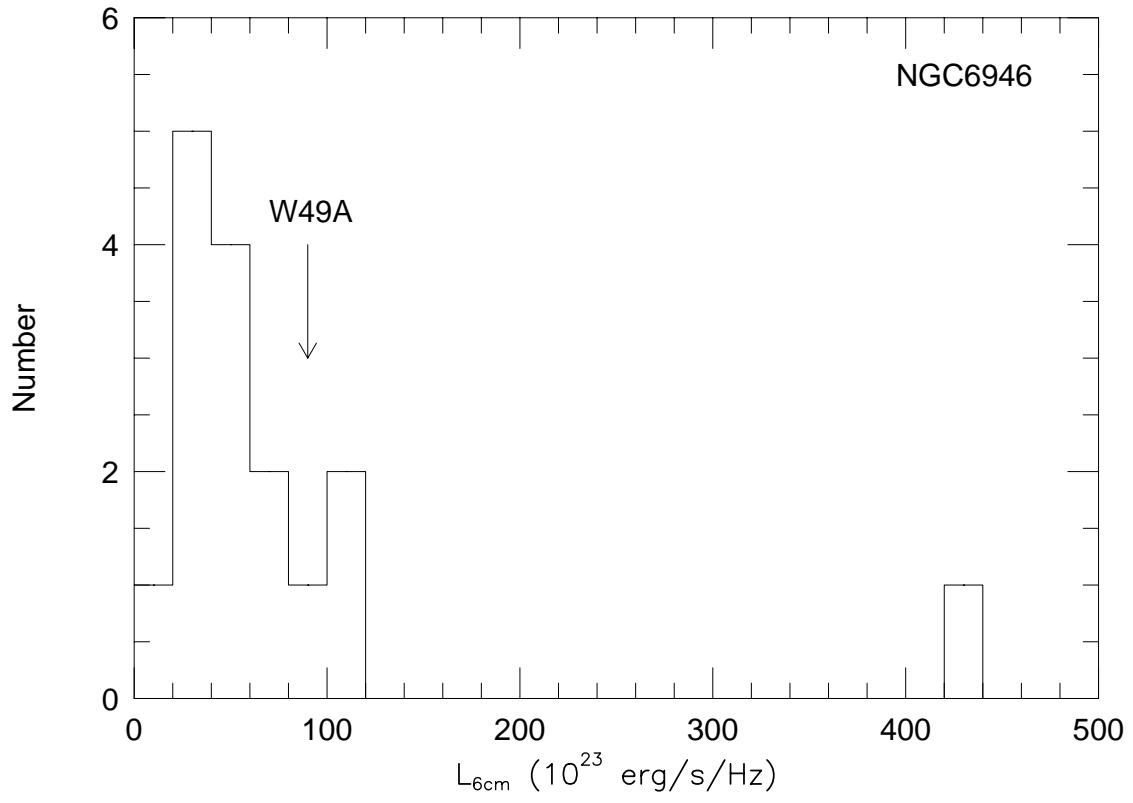


Fig. 8.— A comparison of the luminosity and spectral energy distribution of W49A from Mezger, Schraml, & Terzian (1967) and the *mean* luminosity of UDH II regions from M 33, NGC 253, and NGC 6946. The luminosity and spectral energy distribution of W49A is similar to the UDH II regions in each of the three galaxies in this study.





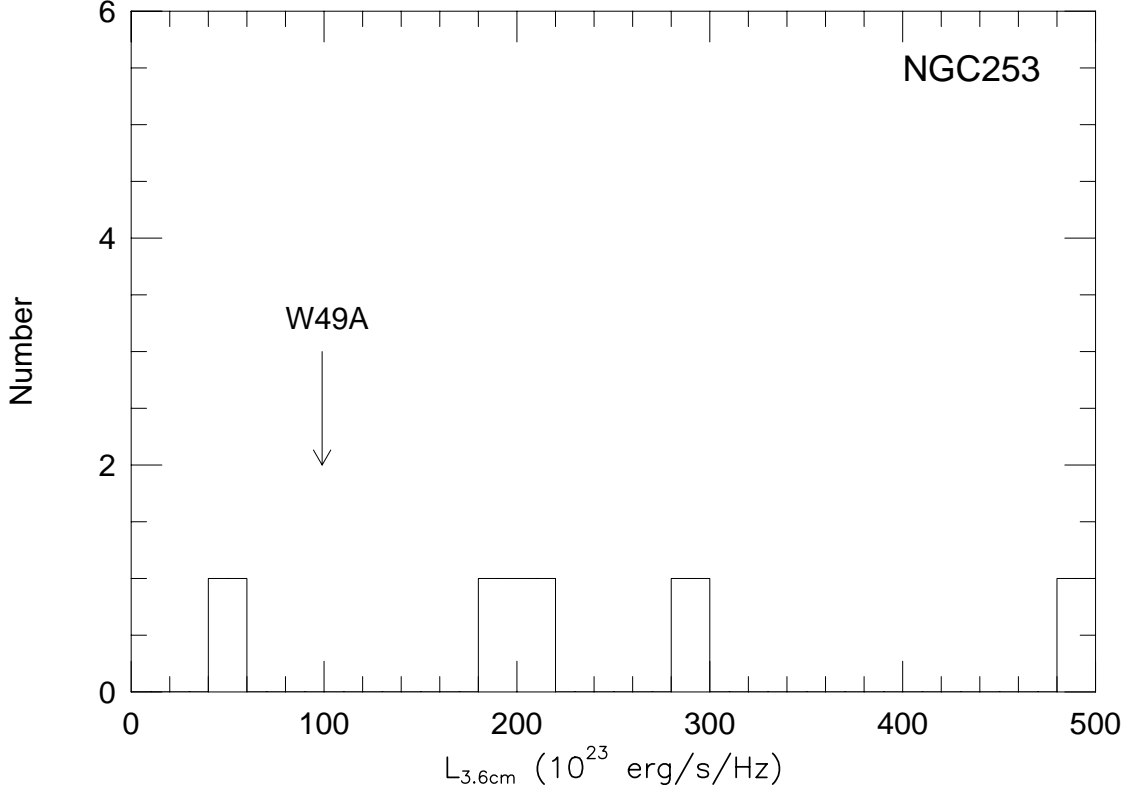


Fig. 9.— Histogram of luminosities for the UDHII candidates for (a) M33, (b) NGC 6946, and (c) NGC 253. The arrow in each plot marks the luminosity of W49A. The dotted line in (a) illustrates the luminosity function of *optically selected* H II regions in M33 from (Smith & Kennicutt 1989) that find  $N(L) \propto L^{-2.3} dL$ . The completeness limit is not well determined, but the  $5\sigma$  noise level is  $\approx 2 \times 10^{23} \text{ erg s}^{-1} \text{ Hz}^{-1}$ .



This figure "fig1a.jpg" is available in "jpg" format from:

<http://arxiv.org/ps/astro-ph/0107181v1>

This figure "fig1b.jpg" is available in "jpg" format from:

<http://arxiv.org/ps/astro-ph/0107181v1>

This figure "fig1c.jpg" is available in "jpg" format from:

<http://arxiv.org/ps/astro-ph/0107181v1>

This figure "fig1d.jpg" is available in "jpg" format from:

<http://arxiv.org/ps/astro-ph/0107181v1>

This figure "fig1e.jpg" is available in "jpg" format from:

<http://arxiv.org/ps/astro-ph/0107181v1>

This figure "fig1f.jpg" is available in "jpg" format from:

<http://arxiv.org/ps/astro-ph/0107181v1>

This figure "fig1g.jpg" is available in "jpg" format from:

<http://arxiv.org/ps/astro-ph/0107181v1>

This figure "fig1h.jpg" is available in "jpg" format from:

<http://arxiv.org/ps/astro-ph/0107181v1>



This figure "fig1i.jpg" is available in "jpg" format from:

<http://arxiv.org/ps/astro-ph/0107181v1>

This figure "fig1j.jpg" is available in "jpg" format from:

<http://arxiv.org/ps/astro-ph/0107181v1>

This figure "fig1k.jpg" is available in "jpg" format from:

<http://arxiv.org/ps/astro-ph/0107181v1>

This figure "fig11.jpg" is available in "jpg" format from:

<http://arxiv.org/ps/astro-ph/0107181v1>

This figure "fig2a.jpg" is available in "jpg" format from:

<http://arxiv.org/ps/astro-ph/0107181v1>

This figure "fig2b.jpg" is available in "jpg" format from:

<http://arxiv.org/ps/astro-ph/0107181v1>

This figure "fig3a.jpg" is available in "jpg" format from:

<http://arxiv.org/ps/astro-ph/0107181v1>

This figure "fig3b.jpg" is available in "jpg" format from:

<http://arxiv.org/ps/astro-ph/0107181v1>



This figure "fig3c.jpg" is available in "jpg" format from:

<http://arxiv.org/ps/astro-ph/0107181v1>

This figure "fig3d.jpg" is available in "jpg" format from:

<http://arxiv.org/ps/astro-ph/0107181v1>

This figure "fig3e.jpg" is available in "jpg" format from:

<http://arxiv.org/ps/astro-ph/0107181v1>

This figure "fig3f.jpg" is available in "jpg" format from:

<http://arxiv.org/ps/astro-ph/0107181v1>

This figure "fig3g.jpg" is available in "jpg" format from:

<http://arxiv.org/ps/astro-ph/0107181v1>

This figure "fig3h.jpg" is available in "jpg" format from:

<http://arxiv.org/ps/astro-ph/0107181v1>

This figure "fig3i.jpg" is available in "jpg" format from:

<http://arxiv.org/ps/astro-ph/0107181v1>

This figure "fig3j.jpg" is available in "jpg" format from:

<http://arxiv.org/ps/astro-ph/0107181v1>



This figure "fig4a.jpg" is available in "jpg" format from:

<http://arxiv.org/ps/astro-ph/0107181v1>

This figure "fig4b.jpg" is available in "jpg" format from:

<http://arxiv.org/ps/astro-ph/0107181v1>